HHS Public Access

Author manuscript

J Nucl Med. Author manuscript; available in PMC 2015 November 01.

Published in final edited form as:

J Nucl Med. 2015 May ; 56(5): 805–811. doi:10.2967/jnumed.114.149054.

Cerenkov Luminescence Imaging for Radiation Dose Calculation of a ^{90}Y-Labeled Gastrin-Releasing Peptide Receptor Antagonist

Christian Lohrmann[1], **Hanwen Zhang**[2], **Daniel L.J. Thorek**[3], **Pooja Desai**[2], **Pat B. Zanzonico**[4], **Joseph O'Donoghue**[4], **Christopher P. Irwin**[2], **Thomas Reiner**[2], **Jan Grimm**[1,5], and **Wolfgang A. Weber**[1,5]

[1]Molecular Imaging and Therapy Service, Department of Radiology, Memorial Sloan Kettering Cancer Center, New York, New York; [2]Radiochemistry and Imaging Sciences Service, Department of Radiology, Memorial Sloan Kettering Cancer Center, New York, New York; [3]Division of Nuclear Medicine, Department of Radiology, Johns Hopkins Medicine, Baltimore, Maryland; [4]Department of Medical Physics, Memorial Sloan Kettering Cancer Center, New York, New York; [5]Molecular Pharmacology and Chemistry Program, Memorial Sloan Kettering Cancer Center, New York, New York

Abstract

^{90}Y has been used to label various new therapeutic radiopharmaceuticals. However, measuring the radiation dose delivered by ^{90}Y is challenging because of the absence of suitable γ emissions and its low abundance of positron emissions. For the treatment of prostate cancer, radiolabeled gastrin-releasing peptide receptor (GRPr) antagonists have yielded promising results in mouse models. In this study, we evaluated whether Cerenkov luminescence imaging (CLI) could be used to determine radiation doses of a ^{90}Y-labeled GRPr antagonist in nude mice.

Methods—Mice bearing subcutaneous prostate cancer xenografts were injected with 0.74–18.5 MBq of the ^{90}Y-labeled GRPr antagonist DOTA-AR and underwent in vivo and ex vivo CLI at 1–48 h after injection. After imaging, animals were sacrificed, their tumors and organs were harvested, and the activity concentration was measured by liquid scintillation counting. In a second set of experiments, Cerenkov photon counts for tumor and kidney on in vivo CLI were converted to activity concentrations using conversion factors determined from the first set of experiments.

Results—^{90}Y-DOTA-AR concentration in the 3 tumor models ranged from 0.5% to 4.8% of the injected activity per gram at 1 h after injection and decreased to 0.05%–0.15 injected activity per gram by 48 h after injection. A positive correlation was found between tumor activity concentrations and in vivo CLI signal (r^2 = 0.94). A similar correlation was found for the renal activity concentration and in vivo Cerenkov luminescence (r^2 = 0.98). Other organs were not distinctly visualized on the in vivo images, but ex vivo CLI was also correlated with the

For correspondence or reprints contact: Christian Lohrmann, Molecular Imaging and Therapy Service, Department of Radiology, Memorial Sloan Kettering Cancer Center, 1275 York Ave., P.O. Box 77, New York, NY. lohrmanl@mskcc.org.

DISCLOSURE

No other potential conflict of interest relevant to this article was reported.

radioactivity concentration (r^2 = 0.35–0.94). Using the time–activity curves from the second experiment, we calculated radiation doses to tumor and kidney of 0.33 ± 0.12 (range, 0.21–0.66) and 0.06 ± 0.01 (range, 0.05–0.08) Gy/MBq, respectively.

Conclusion—CLI is a promising, low-cost modality to measure individual radiation doses of ^{90}Y-labeled compounds non-invasively. The use of Cerenkov imaging is expected to facilitate the development and comparison of ^{90}Y-labeled compounds for targeted radiotherapy.

Keywords

gastrin-releasing peptide receptor; Cerenkov luminescence imaging; targeted radiotherapy; ^{90}Y

The β-emitter ^{90}Y is used for an increasing number of therapeutic radiopharmaceuticals, including the CD20 antibody ibritumomab tiuxetan, the somatostatin receptor ligands DOTATOC and DOTATATE, and microspheres for treatment of liver metastases (1–3). Because of its high β energy (Emax, 2.28 MeV), ^{90}Y can deliver therapeutically effective radiation doses at relatively low activity concentrations. Furthermore, the absence of γ emissions limits radiation exposure of personnel and individuals caring for the patient after radionuclide therapy. However, the lack of γ emission also represents a limitation of ^{90}Y-labeled pharmaceuticals, because quantitation of the activity delivered to the tumor and to dose-limiting normal organs is technically challenging (4). This is true not only for patient studies but also for preclinical studies in animals.

Rationale development of new ^{90}Y-labeled pharmaceuticals requires a comparison of radiation doses to tumor and normal tissues in animal models. To achieve this, the conventional approach is to perform serial biodistribution studies in large cohorts of animals to measure tissue activity concentrations at various time points and to determine the cumulated activity for each tissue of interest. Measuring activity concentrations at a single time point may be misleading because radiopharmaceuticals with different clearance rates and residence times may deliver different radiation doses despite a similar initial uptake. Noninvasive techniques to measure the concentration of ^{90}Y in animals are also needed to correlate the delivered radiation dose with growth inhibition or regression in individual animals.

^{90}Y can be imaged by SPECT of the bremsstrahlung x-rays emitted after the β decay or by PET using positrons generated by internal electron-positron pair production (5,6). However, internal pair production is a rare event, limiting count statistics and requiring long acquisition times. Bremsstrahlung shows a broad, continuous spectrum with maximum x-ray energies of 2.28 MeV and is therefore difficult to image quantitatively using SPECT (7).

An alternative approach to measure β-emitting isotopes is Cerenkov luminescence (CL), a continuous spectrum of light emitted by β particles as they travel through a dielectric medium such as tissue (8,9). This light signal can be detected by sensitive luminescence imaging systems that are used in many laboratories for bioluminescence imaging (10–14). Because the intensity of CL produced is dependent on the energy of the β radiation, ^{90}Y is better suited for Cerenkov luminescence imaging (CLI) than low-energy positron emitters such as ^{18}F. Phantom studies by Liu et al. (15) have shown that ^{90}Y emits about 10 times

more detectable Cerenkov light per radioactive decay than ^{18}F. These investigators have also demonstrated the feasibility of CLI of tumor xenografts with ^{90}Y-labeled peptides (15). An additional advantage of ^{90}Y is the absence of γ emissions, which generate noise in the optical detector system (16). In a recent study, the higher β energy and the lack of γ emissions resulted in an overall 270-fold-higher sensitivity of Cerenkov imaging with ^{90}Y as compared with ^{18}F (16).

The purpose of the present study was therefore to evaluate CLI as a quantitative imaging modality to estimate the radiation dose of ^{90}Y-labeled radiopharmaceuticals in mice. Our hypothesis was that CLI will allow rapid, noninvasive, serial measurements of activity concentrations in situ radiation that can be used to estimate radiation doses to tumor and normal organs. We tested this hypothesis for a ^{90}Y-labeled gastrin-releasing peptide receptor (GRPr or bombesin receptor) antagonist in mice bearing prostate cancer xenografts. Prostate cancer remains the second-leading cause of cancer death in men in the United States (17), hence there remains an enormous need for new therapeutic strategies, especially for locally advanced and metastatic disease.

MATERIALS AND METHODS

The GRPr antagonist DOTA-AR (Fig. 1) was selected on the basis of its excellent GRPr-targeting efficacy and synthesized as previously described by Abiraj et al. (18). ^{90}Y-DOTA-AR was prepared by dissolving 20 μg of peptide (11.4 nmol) in ammonium acetate buffer (200 mL, 0.5 M, pH 5.4) (Fig. 1). The radiochemical yield and purity were typically 80%–90% (decay corrected) and more than 95%, respectively. After the addition of $^{90}YCl_3$ (370 MBq), the solution was incubated for 25 min at 95°C (Fig. 1). A hydrophilic–lipophilic balance cartridge preconditioned with methanol (5 mL) and water (5 mL) was used to remove the free ^{90}Y from the ^{90}Y-DOTA-AR. After hydrophilic-lipophilic balance purification, the radioligand, with a specific activity of 9.62–18.5 MBq/μg, was diluted in 0.9% NaCl with 0.1% bovine serum albumin for in vivo studies.

The GRPr-expressing human prostate cancer cell lines PC-3 (high expression of GRPr), VCaP (high expression of GRPr), and LNCaP (low expression of GRPr) were obtained from American Tissue Culture Collection and cultured in RPMI-1640 medium (MSKCC Media Preparation Facility), supplemented with 10% fetal bovine serum (HyClone) and penicillin (10,000 IU/mL) and streptomycin (10,000 μg/mL).

Experiments were performed according to a protocol approved by the Institutional Animal Care and Use Committee. Xenografts of PC-3, VCaP, and LNCaP cells were established by the subcutaneous injections of 5×10^6 tumor cells suspended in 150 mL of 1:1 respective cell growth medium/Matrigel (BD Biosciences) in the area of the left shoulder of male athymic nude (outbred)/CrTac:NCr-Foxn1nu mice (7–9 wk; weight, ~20 γ each; Taconic). When tumors reached a volume of approximately 150 mm^3 (at 14–28 d after implantation), experiments were performed.

CLI

Fifteen mice bearing PC-3 prostate cancer xenografts were injected into the lateral tail vein with an activity of 11.1 MBq. In vivo and ex vivo CLI was performed at 1, 4, 24, and 48 h after injection. For determination of nonspecific uptake, a group of 3 PC-3 tumor–bearing mice was preinjected (5 min) with 154 nmol of unlabeled GRPr antagonist HZ201 ([D-Phe^6]-BN(6–13)-ethylester) into the lateral tail vein, followed by 2.775 MBq of ^{90}Y-DOTA-AR. To test the feasibility of CLI for other prostate cancer models, we injected groups of 3 mice bearing VCap and LnCAp tumors with 2.775 MBq of ^{90}Y-DOTA-AR and performed in vivo and ex vivo imaging at 4 h after injection.

For in vivo imaging, CLI mice were anesthetized with isoflurane (1%–4%). CL images of 5-min duration were acquired with an IVIS 200 scanner (Caliper Life Sciences). For quantification of CLI signals, regions of interest were placed over the tumor and kidneys, which were both well visualized on the CL images. After the in vivo scan, the mice were sacrificed and dissected. Tumors and organs were placed in a tissue culture dish for ex vivo CLI, which was performed using the same scanner and acquisition parameters as for in vivo CLI. Regions of interest were manually drawn around tumors and normal organs on the in vivo and ex vivo images. CL intensity was expressed as average radiance in number of photons (p) per second (s) per surface area (cm^2) per steradian (sr), that is, p/s/cm^2/sr.

After in vivo and ex vivo CLI, tumor and normal tissues were weighed, solubilized overnight in 1 mL of a SOLVABLE tissue solubilizer (PerkinElmer), and diluted to 5 mL with a commercial scintillation fluid cocktail (Insta-Fluor Plus; PerkinElmer) for liquid scintillation counting (LCS) (Tri-Carb 2910TR; PerkinElmer). The total counts injected per animal were determined by extrapolation from counts of an aliquot taken from the injected solution. The biodistribution data were expressed as percentage injected activity per gram of tissue (%IA/g).

Because we observed a linear relationship of the LCS-derived activity concentrations and the CL light signal with no obvious intercept (Fig. 2), we used linear regression to calculate a calibration factor, K, for conversion of radiance to activity concentration:

$$\text{Activity concentration}[\text{MB q/g}]=\text{K}\times\text{radiance}[(\text{p/s/cm}^2\text{/sr})].$$

Absorbed Dose Calculations

To evaluate the ability to measure individual tumor time–activity curves by CLI, 14 mice bearing PC-3 tumors were divided into 5 groups, and ^{90}Y-DOTA-AR was injected into the lateral tail vein with an activity of 0.74, 1.85, 3.7, 7.4, and 18.5 MBq (injected amount 0.02–0.57 nmol). In vivo CLI was performed in each group at 4, 24, 48, and 72 h after injection of ^{90}Y-DOTA-AR. The measured photon counts for Cerenkov radiation (CR) were converted to activity concentrations using the conversion factors determined in the experiments described above.

From these data, the ^{90}Y tumor- and kidney-absorbed doses (Gy/MBq) were derived as follows. The tumor and kidney time–activity data (%IA/g) were fit to biexponential

functions, and the resulting functions were analytically integrated, incorporating the effect of the physical decay of the ^{90}Y to derive the respective residence times (MBq h/g/MBq). The resulting residence time was then multiplied by the ^{90}Y equilibrium dose constant for nonpenetrating radiations (i.e., β particles), 0.538 g-Gy/MBq-h. To correct for partial absorption of β particles, these doses were multiplied by a volume-based absorbed fraction to calculate absorbed doses (Gy/MBq) to the tumor and kidney. Tumor and kidney volumes were derived from the 2-dimensional area on the white light images assuming ellipsoid geometry. Absorbed fractions for ^{90}Y were taken from data published by Bardiès and Chatal (19).

RESULTS

The biodistribution of ^{90}Y-DOTA-AR in tumor-bearing nude mice is briefly summarized in Table 1 and shown in detail in Supplemental Table 1 (supplemental materials are available at http://jnm.snmjournals.org). Activity concentrations in PC-3 tumors (mean ± SD) were 3.62 ± 0.95 %IA/g at 1 h and 2.92 ± 0.57 %IA/g at 4 h, with washout by later time points (0.45 ± 0.04 %IA/g at 24 h; 0.10 6± 0.05 %IA/g at 48 h).

The pancreas, kidneys, and lung were the organs with the highest activity concentrations at the 1-h time point (Supplemental Table 1). Except for the lung, all normal organs showed washout of activity at the 4-h time point, resulting in increased tumor–to– normal organ ratios at the 4-h time point. ^{90}Y-DOTA-AR demonstrated a fast blood clearance, with only 0.03 ± 0.03 %IA/g remaining in the blood at 4 h after injection.

The ex vivo CLI radiance data for ^{90}Y-DOTA-AR (Table 2; Figs. 2A and 2B) show the same pattern as the activity concentration measurements. Furthermore, linear regression analysis generally demonstrated a close correlation between ^{90}Y-DOTA-AR activity concentration (%IA/g) and ex vivo CR (p/s/cm^2/sr). For example, the correlation coefficient (R^2) between ex vivo CLI radiance and activity concentration was 0.91 for PC-3 tumors (Fig. 2A) and 0.99 for kidneys (Fig. 2B). Figure 3 shows an example of ex vivo CLI at 4 h. Correlations between ex vivo CLI and activity concentrations for other organs are shown in Supplemental Figure 2.

The tumor and kidneys were also visualized by in vivo CLI (Fig. 3). For both tissues, there was a significant correlation between in vivo CLI radiance and ex vivo activity concentrations (PC-3 tumors, $R^2 = 0.94$; kidneys, $R^2 = 0.98$) (Figs. 2C and 2D). The slope of the regression line was 2.9×10^{25} (%IA/g)/(p/s/cm^2/sr) or 3.145×10^{26} (MBq/g)/(p/s/cm^2/sr) for the tumors and 2.4×10^{25} (%IA/g)/(p/s/cm^2/sr) or 2.627×10^{26} (MBq/g)/(p/s/cm^2/sr) for the kidneys.

As expected, LNCaP tumors demonstrated a low CL, whereas uptake by VCaP tumors was comparable to PC-3, reflecting the relative GRPr expression levels of the 3 tumor cell lines; the CL correlated to a marked difference in radioactivity concentrations between LNCaP and VCaP tumors (Tables 1 and 2; Fig. 4). Cerenkov imaging was also able to document blocking of the binding of radiolabeled ^{90}Y-DOTA-AR with an unlabeled GRPr ligand (Fig. 5). Both the Cerenkov signal and radioactivity concentrations were reduced by about 80%

by preinjection of an approximately 300-fold excess of the unlabeled GRPr antagonist HZ201(Fig. 5).

Figure 6A shows an example of a mouse that was imaged by CLI at various time points after injection of 0.74 MBq of ^{90}Y-DOTA-AR. Both tumors and kidneys were visualized for injected activities ranging from 0.74 MBq to 18.5 MBq at 4 and 24 h after injection. At later time points, the kidney was only visible for mice that had been injected with at least 3.7 MBq. Using these serial images and the calibration factors from the previous set of experiments, we estimated the radioactivity concentration in the tumor and the kidneys over time (Figs. 6B, 6C, and 7). A dose-dependent decrease of the %IA/g in the tumor with increasing administered activities was apparent; presumably, the receptors are partially saturated at higher injected activities/peptide masses. No such effect was observed for the kidneys, which do not express GRPrs. Overall, tumor doses showed a more than 3-fold variability and ranged from 0.21 to 0.66 Gy/MBq. Renal doses were also variable and ranged from 0.05 to 0.08 Gy/MBq. The calculated absorbed fraction doses to tumor and kidneys of individual animals are shown in Table 3.

DISCUSSION

The success of peptide receptor-targeted radiotherapy in neuroendocrine tumors (2) has renewed the interest in treating cancer with β-emitting radioisotopes. Radioloabeled GRPr antagonists have shown promise for the treatment of prostate cancer in preclinical studies because of their favorable biodistribution and high tumor uptake (20–26). These findings were confirmed in the present study, which demonstrated a similar biodistribution profile of the GRPr antagonist ^{90}Y-DOTA-AR, as previously reported for other radiolabeled GRPr antagonists (18,22,25).

The biodistribution of radiopharmaceuticals is influenced by multiple factors, including target density, regional perfusion, vascular permeability, and renal and hepatic function. These parameters may well differ among individual animals and can change over time within an individual animal. Furthermore, labeling of the same molecule with different isotopes can markedly affect target binding affinity. For example, the affinity of ^{68}Ga-DOTATOC for the somatostatin type 2 receptor is more than 4-fold higher than that of ^{90}Y-DOTATOC (27). Therefore, it can be difficult to predict the uptake of a ^{90}Y-labeled peptide based on the uptake of the same peptide labeled with a different radiometal. Thus, it is desirable to directly measure concentrations of ^{90}Y during therapy both noninvasively and repetitively.

One approach to achieve this goal is to visualize and quantify the CL of ^{90}Y. The proof-of-principle work by Robertson et al. (28) used CLI in vitro and in vivo to image human prostate cancer xenografts after injection of different β-emitting radioisotopes. Several reports followed and demonstrated successfully the application of optical imaging with β^+ and β^- emitters (10–13,16,17,29,30) in preclinical models. CLI has also been used clinically during therapy of hyperthyroidism with ^{131}I (31). Recently, it has been shown that CLI with ^{18}F-FDG allows detection of superficial lymph node metastases in patients (32).

However, CLI is especially promising for imaging during therapy with ^{90}Y, because the amount of Cerenkov photons is dependent on the β energy. Although ^{18}F (β^+ with a positron endpoint energy of 633 keV) will create 1.4 photons per decay (in water), ^{90}Y (β^- with an endpoint energy of 2.28 MeV) can produce up to 57 photons per decay (29,33). The wavelength of CL lies mostly within the visible and ultraviolet part of the spectrum, which leads to strong attenuation in tissue. Furthermore, the scanning must be performed while carefully excluding external light sources because of the low overall amount of available photons, requiring low background photon counts. However, this procedure does not present a major obstacle for imaging subcutaneous tumors in nude mice, with widely available systems for bioluminescence imaging—a technique that also requires acquisition without ambient light.

In the present study, we show a close correlation between ex vivo CLI and radioactivity concentrations measured by LCS. Ex vivo CLI is much less time-consuming than LCS, which requires tissue homogenization. Therefore, CLI could facilitate comparison of the biodistribution of different ^{90}Y-labeled radiotracers in mice. More important, we also found a close correlation between in vivo CLI and concentration of ^{90}Y in subcutaneous tumors, allowing us to confirm receptor-specific uptake of the ^{90}Y-labeled peptide by blocking studies and in vivo imaging. We were also able to non-invasively study the effect of increasing peptide mass on tumor activity concentrations. Finally, serial CLI studies allowed us to noninvasively estimate the radiation dose for tumors and kidneys in individual mice. This noninvasive estimation represents a significant advantage over conventional biodistribution studies that pool data from multiple animals. To our knowledge, CLI is the only modality capable of this kind of in vivo characterization of ^{90}Y-labeled peptides in such a facile and cost-effective way, as data of up to 5 animals can be acquired simultaneously within 5 min.

An alternative to CLI of ^{90}Y-labeled compounds is PET with ^{86}Y (34). However, average PET examination times in a preclinical setting account for approximately 20 min per mouse. Hence, many more mice can be evaluated using CLI than PET. Furthermore, ^{86}Y is an expensive radioisotope and is not commonly available, significantly limiting the ability to perform larger studies using ^{86}Y PET.

Although the findings of our study are encouraging for the use of CLI during preclinical development of ^{90}Y-labeled pharmaceuticals, the following limitations should be noted. Although superficial tumors and kidneys were well visualized by CLI, more deep-seated organs, such as the pancreas, could not be delineated by CLI. Thus, the ability of CLI to noninvasively estimate doses to deep-seated normal organs or orthotopic tumors appears limited. For radiopeptides, however, the kidney is frequently the dose-limiting organ. Therefore, we expect that CLI can provide important information for the development of many ^{90}Y-labeled peptides.

It is also important to note that the rapid clearance of ^{90}Y-DOTA-AR resulted in low background activity concentrations, which facilitated visualization of tumors and quantification of intratumoral activity concentrations. Future studies are required to assess the accuracy of quantitative CLI for radiopharmaceuticals with less-selective tumor

targeting. However, therapeutic radiopharmaceuticals will generally require high tumor–to–normal organ ratios and it is therefore likely that CLI will allow the quantitative assessment of intratumoral activity concentrations for other therapeutic radiopharmaceuticals as well.

Because of the short range of CL, the intensity of the CLI signal is mainly determined by the activity concentration at the surface of a tumor. Consequently, CLI will overestimate the total activity concentration in tumors with necrotic centers. For the same reasons, the tumor CL signal is dependent on the positioning of the animals, thus necessitating standardization for imaging studies.

CONCLUSION

CLI is a promising, low-cost modality to measure individual radiation doses by ^{90}Y-labeled peptides for tumor xenografts and kidneys in mice. The use of Cerenkov imaging is expected to facilitate the development and comparison of b emitters for targeted radiotherapy.

Supplementary Material

Refer to Web version on PubMed Central for supplementary material.

Acknowledgments

We gratefully acknowledge the staff of the MSK Small Animal Imaging Core Facility. The authors also thank Leah Bassity for her editorial work on the manuscript.

This study was supported in part by the R25T Molecular Imaging Fellowship “Molecular Imaging Training in Oncology” (5R25CA096945-07) and by the NIH (1R01EB01494). J.G. was additionally supported by a NIBIB award 5R01EB014944-03 and NCI award 1R01CA183953. Technical services provided by the MSK Small Animal Imaging Core Facility were supported in part by NIH Cancer Center Support grant 2 P30 CA008748-48.

References

1. Morschhauser F, Radford J, Van Hoof A, et al. ^{90}Yttrium-ibritumomab tiuxetan consolidation of first remission in advanced-stage follicular non-Hodgkin lymphoma: updated results after a median follow-up of 7.3 years from the International, Randomized, Phase III First-Line Indolent Trial. J Clin Oncol. 2013; 31:1977–1983. [PubMed: 23547079]
2. Ambrosini V, Fani M, Fanti S, Forrer F, Maecke HR. Radiopeptide imaging and therapy in Europe. J Nucl Med. 2011; 52(suppl 2):42S–55S. [PubMed: 22144555]
3. Evans KA, Richardson MG, Pavlakis N, et al. Survival outcomes of a salvage patient population after radioembolization of hepatic metastases with yttrium-90 microspheres. J Vasc Interv Radiol. 2010; 21:1521–1526. [PubMed: 20813542]
4. Rong X, Du Y, Ljungberg M, Rault E, Vandenberghe S, Frey EC. Development and evaluation of an improved quantitative ^{90}Y bremsstrahlung SPECT method. Med Phys. 2012; 39:2346–2358. [PubMed: 22559605]
5. Minarik D, Sjögreen-Gleisner K, Linden O, et al. ^{90}Y Bremsstrahlung imaging for absorbed-dose assessment in high-dose radioimmunotherapy. J Nucl Med. 2010; 51:1974–1978. [PubMed: 21078799]
6. Elschot M, Vermolen BJ, Lam MG, de Keizer B, van den Bosch MA, de Jong HW. Quantitative comparison of PET and Bremsstrahlung SPECT for imaging the in vivo yttrium-90 microsphere distribution after liver radioembolization. PLoS ONE. 2013; 8:e55742. [PubMed: 23405207]

7. Rong X, Du Y, Frey EC. A method for energy window optimization for quantitative tasks that includes the effects of model-mismatch on bias: application to Y-90 bremsstrahlung SPECT imaging. Phys Med Biol. 2012; 57:3711–3725. [PubMed: 22617760]
8. Cherenkov PA. Visible emission of clean liquids by action of gamma-radiation. Dokl Akad Nauk SSSR. 1934; 2:451–452.
9. Thorek DLJ, Robertson R, Bacchus WA, et al. Cerenkov imaging: a new modality for molecular imaging. Am J Nucl Med Mol Imaging. 2012; 2:163–173. [PubMed: 23133811]
10. Ruggiero A, Holland JP, Lewis JS, Grimm J. Cerenkov luminescence imaging of medical isotopes. J Nucl Med. 2010; 51:1123–1130. [PubMed: 20554722]
11. Spinelli AE, D'Ambrosio D, Calderan L, Marengo M, Sbarbati A, Boschi F. Cerenkov radiation allows in vivo optical imaging of positron emitting radio-tracers. Phys Med Biol. 2010; 55:483–495. [PubMed: 20023328]
12. Holland JP, Normand G, Ruggiero A, Lewis JS, Grimm J. Intraoperative imaging of positron emission tomographic radiotracers using Cerenkov luminescence emissions. Mol Imaging. 2011; 10:177–186. [PubMed: 21496448]
13. Liu H, Carpenter CM, Jiang H, et al. Intraoperative imaging of tumors using Cerenkov luminescence endoscopy: a feasibility experimental study. J Nucl Med. 2012; 53:1579–1584. [PubMed: 22904353]
14. Chin PT, Welling MM, Meskers SC, Valdes Olmos RA, Tanke H, van Leeuwen FW. Optical imaging as an expansion of nuclear medicine: Cerenkov-based luminescence vs fluorescence-based luminescence. Eur J Nucl Med Mol Imaging. 2013; 40:1283–1291. [PubMed: 23674205]
15. Liu H, Ren G, Miao Z, et al. Molecular optical imaging with radioactive probes. PLoS ONE. 2010; 5:e9470. [PubMed: 20208993]
16. Carpenter CM, Ma X, Liu H, et al. Cerenkov luminescence endoscopy: improved molecular sensitivity with b-emitting radiotracers. J Nucl Med. 2014; 55:1905–1909. [PubMed: 25300598]
17. Siegel R, Ma J, Zou Z, Jemal A. Cancer statistics, 2014. CA Cancer J Clin. 2014; 64:9–29. [PubMed: 24399786]
18. Abiraj K, Mansi R, Tamma ML, et al. Bombesin antagonist-based radioligands for translational nuclear imaging of gastrin-releasing peptide receptor-positive tumors. J Nucl Med. 2011; 52:1970–1978. [PubMed: 22080443]
19. Bardiès M, Chatal JF. Absorbed doses for internal radiotherapy from 22 beta-emitting radionuclides: beta dosimetry of small spheres. Phys Med Biol. 1994; 39:961–981. [PubMed: 15551573]
20. Mansi R, Wang X, Forrer F, et al. Evaluation of a 1,4,7,10-tetraazacyclododecane-1,4,7,10-tetraacetic acid-conjugated bombesin-based radioantagonist for the labeling with single-photon emission computed tomography, positron emission tomography, and therapeutic radionuclides. Clin Cancer Res. 2009; 15:5240–5249. [PubMed: 19671861]
21. Schroeder RP, Müller C, Reneman S, et al. A standardised study to compare prostate cancer targeting efficacy of five radiolabelled bombesin analogues. Eur J Nucl Med Mol Imaging. 2010; 37:1386–1396. [PubMed: 20182713]
22. Mansi R, Wang X, Forrer F, et al. Development of a potent DOTA-conjugated bombesin antagonist for targeting GRPr-positive tumours. Eur J Nucl Med Mol Imaging. 2011; 38:97–107. [PubMed: 20717822]
23. Lears KA, Ferdani R, Liang K, et al. In vitro and in vivo evaluation of ^{64}Cu-labeled SarAr-bombesin analogs in gastrin-releasing peptide receptor-expressing prostate cancer. J Nucl Med. 2011; 52:470–477. [PubMed: 21321264]
24. Yang M, Gao H, Zhou Y, et al. F-labeled GRPR agonists and antagonists: a comparative study in prostate cancer imaging. Theranostics. 2011; 1:220–229. [PubMed: 21544226]
25. Dumont RA, Tamma M, Braun F, et al. Targeted radiotherapy of prostate cancer with a gastrin-releasing peptide receptor antagonist is effective as monotherapy and in combination with rapamycin. J Nucl Med. 2013; 54:762–769. [PubMed: 23492884]
26. Mansi R, Fleischmann A, Mäcke HR, Reubi JC. Targeting GRPR in urological cancers: from basic research to clinical application. Nat Rev Urol. 2013; 10:235–244. [PubMed: 23507930]

27. Reubi JC, Schar JC, Waser B, et al. Affinity profiles for human somatostatin receptor subtypes SST1-SST5 of somatostatin radiotracers selected for scinti-graphic and radiotherapeutic use. Eur J Nucl Med. 2000; 27:273–282. [PubMed: 10774879]

28. Robertson R, Germanos MS, Li C, Mitchell GS, Cherry SR, Silva MD. Optical imaging of Cerenkov light generation from positron-emitting radiotracers. Phys Med Biol. 2009; 54:N355–N365. [PubMed: 19636082]

29. Mitchell GS, Gill RK, Boucher DL, Li C, Cherry SR. In vivo Cerenkov luminescence imaging: a new tool for molecular imaging. Philos Transact A Math Phys Eng Sci. 2011; 369:4605–4619.

30. Thorek DLJ, Ogirala A, Beattie BJ, Grimm J. Quantitative imaging of disease signatures through radioactive decay signal conversion. Nat Med. 2013; 19:1345–1350. [PubMed: 24013701]

31. Spinelli AE, Ferdeghini M, Cavedon C, et al. First human Cerenkography. J Biomed Opt. 2013; 18:20502. [PubMed: 23334715]

32. Thorek DLJ, Riedl CC, Grimm J. Clinical Cerenkov luminescence imaging of ^{18}F-FDG. J Nucl Med. 2014; 55:95–98. [PubMed: 24078721]

33. Beattie BJ, Thorek DLJ, Schmidtlein CR, Pentlow KS, Humm JL, Hielscher AH. Quantitative modeling of Cerenkov light production efficiency from medical radionuclides. PLoS ONE. 2012; 7:e31402. [PubMed: 22363636]

34. Nayak TK, Brechbiel MW. 86Y based PET radiopharmaceuticals: radiochemis-try and biological applications. Med Chem. 2011; 7:380–388. [PubMed: 21711222]

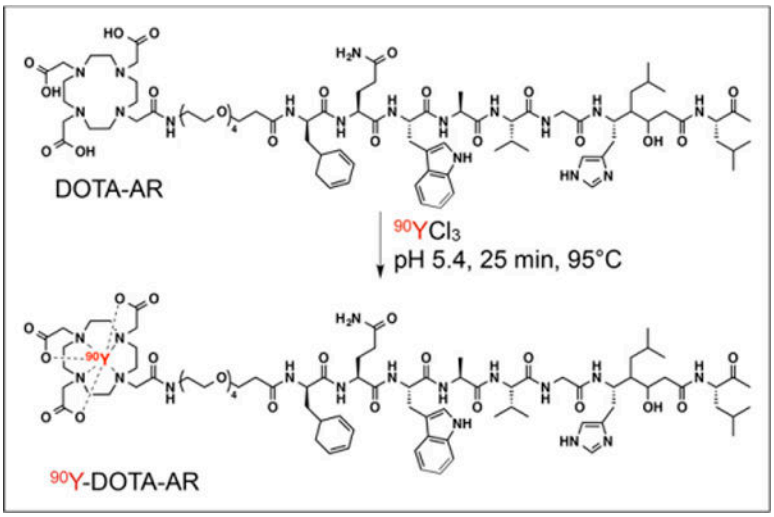

FIGURE 1.
Structure of ^{90}Y-DOTA-AR.

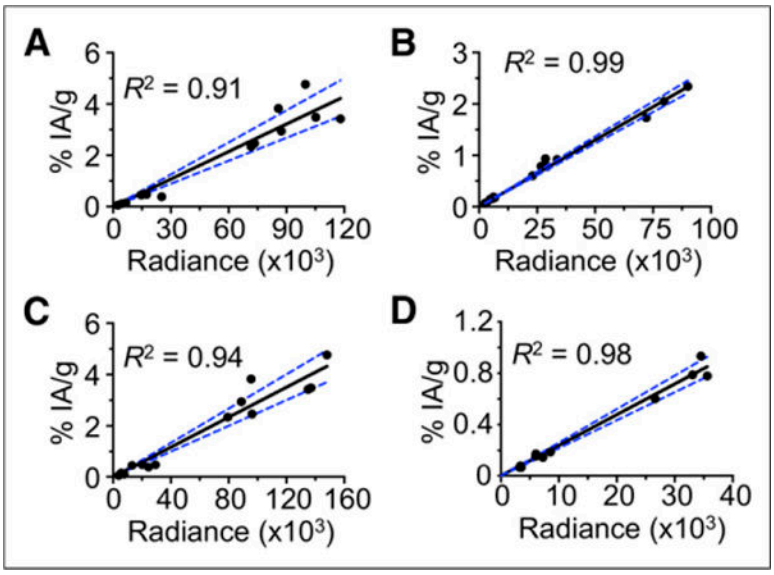

FIGURE 2.

Correlation of CLI radiance (p/s/cm^2/sr) and %IA/g in PC-3 tumor–bearing mice injected with 11.1 MBq of ^{90}Y-DOTA-AR. (A) Ex vivo data tumor. (B) Ex vivo data kidney. (C) In vivo data tumor. (D) In vivo data kidney. Graphs include data from tissues sampled from 1 to 48 h after injection.

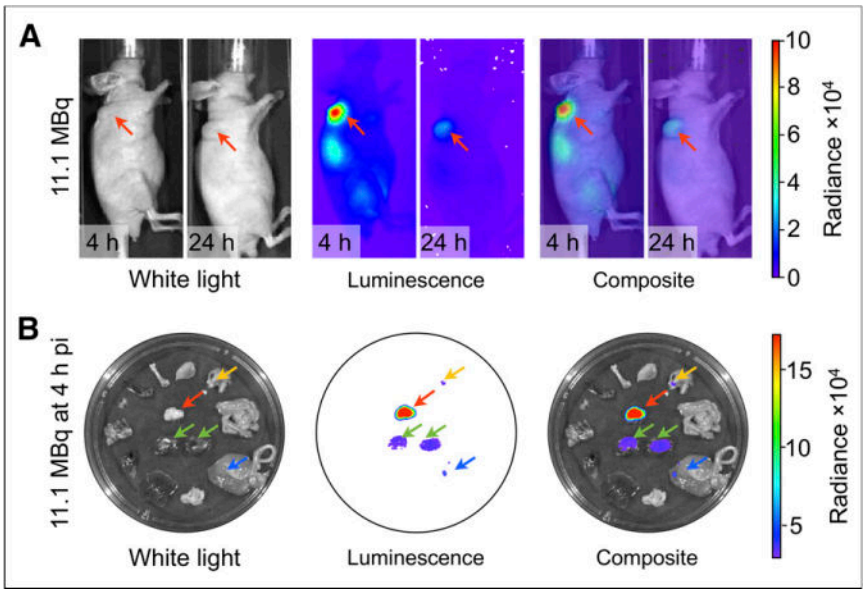

FIGURE 3.

CLI of ^{90}Y-DOTA-AR in PC-3 tumor–bearing nude mice. (A) Tumors in area of left shoulder (in vivo white light images) demonstrate high radiance (p/s/cm^2/sr) at 4 after injection and moderate radiance at 24 h after injection. Kidney is also well visualized on 4-h images. (B) Ex vivo images of 4 h after injection clearly delineate radiance for tumor, kidneys, and in some organs not seen on in vivo images due to absorption of CL signal. Green arrows 5 kidneys; yellow arrow = stomach; blue arrow = large intestine; red arrow = tumor. pi = after injection.

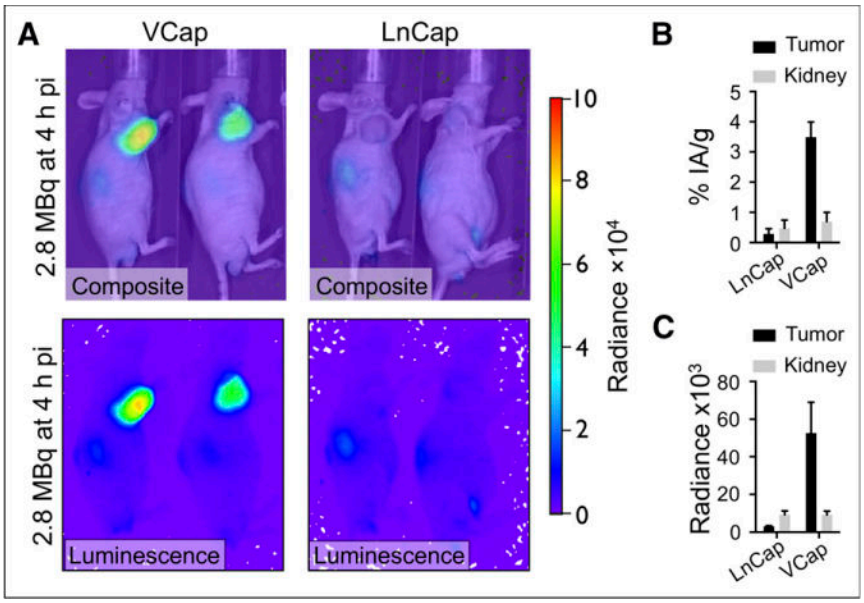

FIGURE 4.

CLI of ^{90}Y-DOTA-AR in representative VCaP and LNCaP tumor–bearing nude mice. (A) Tumors in area of left shoulder demonstrate high radiance in VCaP and low radiance in LNCaP tumors on in vivo luminescence and composite images. (B) Graph demonstrates %IA/g for VCaP (n = 3) and LNCaP (n = 2) tumors. (C) Graph demonstrates radiance for VCaP (n = 3) and LNCaP (n = 2) tumors. Radiance is expressed in p/s/cm2/sr. pi 5 after injection.

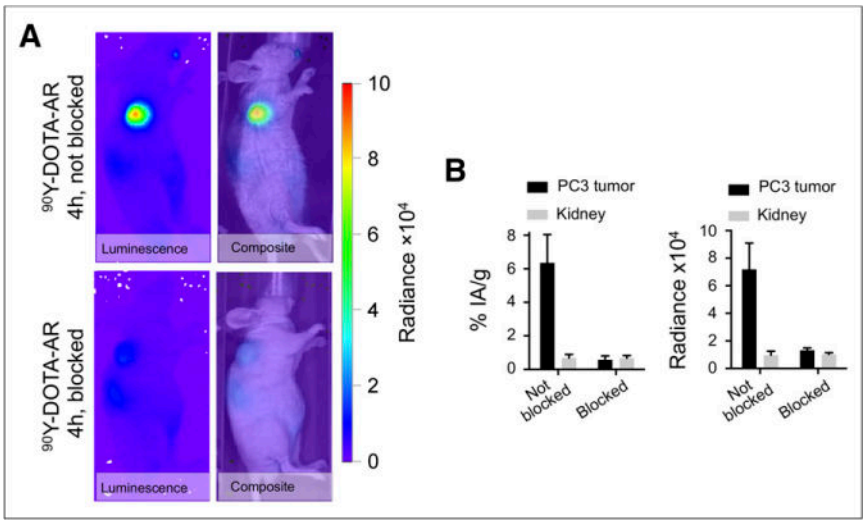

FIGURE 5.

(A) CLI in blocked and nonblocked PC-3 tumor–bearing representative nude mice after injection of ^{90}Y-DOTA-AR. Tumors in area of left shoulder demonstrate high radiance in nonblocked tumors and low radiance in blocked tumors on in vivo luminescence and composite images. (B) Graphs demonstrate %IA/g and radiance for blocked (n = 3) and nonblocked (n = 3) tumors. Radiance is expressed in p/s/cm2/sr.

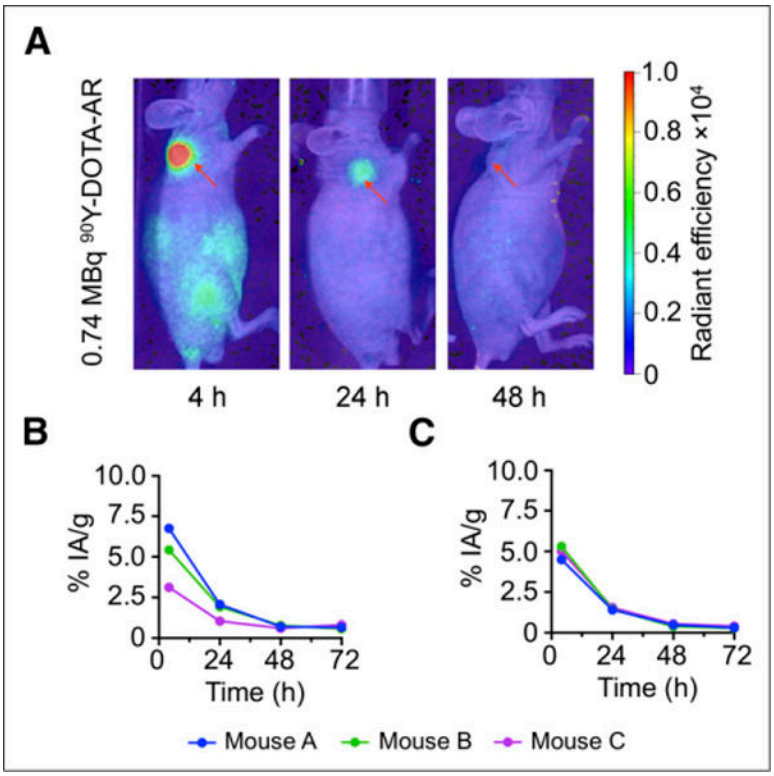

FIGURE 6.

Time course of CLI in representative PC-3 tumor–bearing mouse after injection of 0.74 MBq of ^{90}Y-DOTA-AR. (A) In vivo composite CLI clearly demonstrates high radiance (p/s/cm2/sr) in PC-3 tumor at 4 h and still moderate radiance at 24 h after injection (red arrow). No increased CR signal was detected at 48 h after injection time point (red arrow). Corresponding CLI-based calculated time–activity curves for individual mice with injected doses of 0.74 MBq (B) and 7.4 MBq (C) of radioactivity. Percentage of activity accumulated by tumor decreases for higher injected activity due to partial blocking of receptor by higher injected peptide mass.

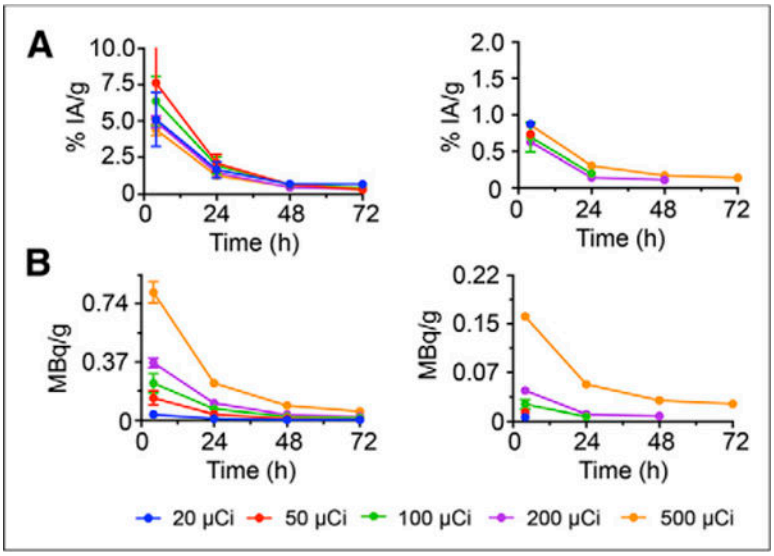

FIGURE 7.

PC-3 tumors and kidneys in mice (n = 14) injected with 0.74–18.5 MBq of ^{90}Y-DOTA-AR. (A) Calculated time–activity (%IA/g) curves for tumors (left) and kidneys (right). (B) Calculated time–activity (MBq/g) curves for tumors (left) and kidneys (right).

TABLE 1

Biodistribution Data of ^{90}Y-DOTA-AR in Nude Mice Bearing Tumors

Organ	1 h	4 h	24 h	48 h
Tumor				
PC-3	3.62 ± 0.95	2.92 ± 0.57	0.45 ± 0.04	0.10 ± 0.05
LNCaP		0.29 ± 0.16		
VCaP		3.49 ± 0.50		
Liver	0.21 ± 0.05	0.12 ± 0.06	0.04 ± 0.01	0.02 ± 0.00
Kidney	1.76 ± 0.61	0.78 ± 0.14	0.17 ± 0.02	0.07 ± 0.01

Data are mean ± SD (%IA/g).

TABLE 2

Ex Vivo CLI Radiance of ^{90}Y-DOTA-AR in Nude Mice Bearing Tumors

Organ	1 h	4 h	24 h	48 h
Tumor				
PC-3	92,779 ± 1,886	84,050 ± 1,604	14,087 ± 3,776	2,658 ± 1,267
LNCaP		2,808 ± 500		
VCaP		52,941 ± 19,524		
Liver	7,324 ± 1,948	3,885 ± 1,751	1,368 ± 217	681 ± 118
Kidney	67,834 ± 2,429	25,650 ± 2,661	4,513 ± 629	1,663 ± 201

Radiance is expressed in p/s/cm^2/sr.

TABLE 3

Absorbed Fraction Doses (Gy/MBq) of ^{90}Y-DOTA-AR in Tumors/Kidneys

Mouse no.	Injected activity (MBq)	Peptide mass (ng)	Tumor	Kidney
1	0.74	40	0.45	
2	0.74	40	0.35	
3	0.74	40	0.21	
			0.34 (average)	
4	1.85	100	0.66	
5	1.85	100	0.36	
6	1.85	100	0.26	
			0.43 (average)	
7	3.7	200	0.26	0.05
8	3.7	200	0.36	0.05
9	3.7	200	0.44	0.07
			0.35 (average)	0.06 (average)
10	7.4	400	0.24	0.05
11	7.4	400	0.22	0.05
12	7.4	400	0.25	0.04
			0.24 (average)	0.05 (average)
13	18.5	1,000	0.23	0.08
14	18.5	1,000	0.28 0.26 (average)	0.06 0.07 (average)